Defining Requirements for Heme Binding in PGRMC1 and Identifying Key Elements that Influence Protein Dimerization

*Prajakta Badve and Katlyn K. Meier**

Department of Chemistry, University of Miami, Coral Gables, FL, 33146, United States

For Table of Contents use only

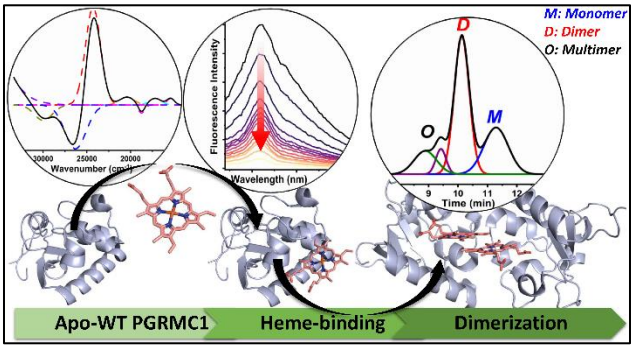

ABSTRACT. Progesterone receptor membrane component 1 (PGRMC1) binds heme via a surface-exposed site and displays some structural resemblance to cytochrome b5 despite their different functions. In the case of PGRMC1, it is the protein interaction with drug-metabolizing cytochrome P450s (CYPs) and the epidermal growth factor receptor (EGFR) that has garnered the most attention. These interactions are thought to result in a compromised ability to metabolize common chemotherapy agents and to enhance cancer cell proliferation. X-ray crystallography and immunoprecipitation data have suggested that heme-mediated PGRMC1 dimers are important in facilitating these interactions. However, more recent studies have called into question the

requirement of heme binding for PGRMC1 dimerization. Our study employs spectroscopic and computational methods to probe and define heme binding and its impact on PGRMC1 dimerization. Fluorescence, electron paramagnetic resonance (EPR) and circular dichroism (CD) spectroscopies confirm heme binding to apo-PGRMC1 and were used to demonstrate the stabilizing effect of heme on the wild-type protein. We also utilize variants (C129S and Y113F) to precisely define the contributions of disulfide bonds and direct heme coordination to PGRMC1 dimerization. Understanding the key factors involved in these processes has important implications for downstream protein-protein interactions that may influence the metabolism of chemotherapeutic agents. This work opens avenues for deeper exploration into the physiological significance of the truncated-PGRMC1 model and for developing design principles for potential therapeutics to target PGRMC1 dimerization and downstream interactions.

INTRODUCTION.

Progesterone receptor membrane component 1 (PGRMC1) is a member of the membrane-associated progesterone receptor (MAPR) protein family, and it contains a heme-binding domain resembling that of Cytochrome b_5.[1-14] PGRMC1 is highly expressed in heme-rich organs such as breast, liver, and ovaries,[2, 4-8, 12, 14] suggesting its involvement in diverse functions including membrane trafficking[11-13, 15], drug, hormone and lipid metabolism[5, 7, 12, 13, 15-21], apoptosis regulation[13, 15, 22], glucose-stimulated insulin release from beta cells[13, 15], steroidogenesis[6, 13, 15], systemic iron homeostasis[13, 15, 23], and even amyloid beta accumulation in neurons[12, 24]. Over the past decade, immunoprecipitation and Western blotting studies have revealed that PGRMC1, when loaded with heme, interacts with downstream epidermal growth factor receptor (EGFR) and drug-metabolizing cytochromes P450 (CYPs).[12, 25, 26] However, the detailed nature of these interactions remains unclear, and requires further study to understand their structural characteristics and

functional roles. PGRMC1 is of particular importance due to its association with enhanced tumor cell proliferation, overexpression in multiple types of cancers and increased resistance to common chemotherapeutic agents.[10, 27-31] Understanding these links can provide valuable insights into the role of PGRMC1 in cancer progression and drug metabolism.

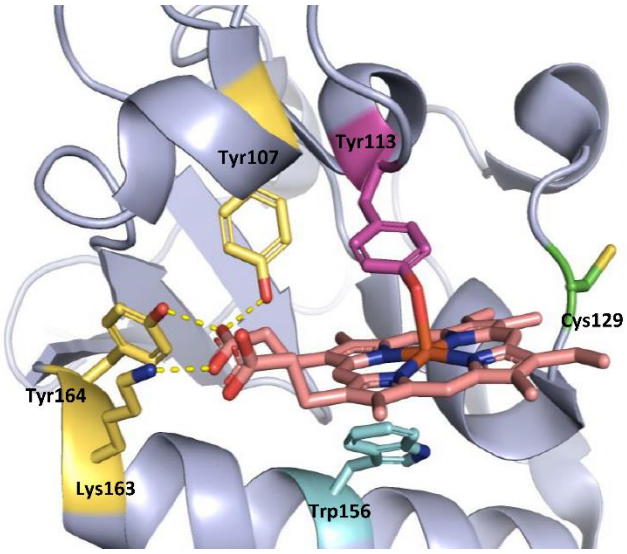

Figure 1. Heme (salmon) binding site in PGRMC1. Tyr113 (magenta) coordinates iron (Fe) (orange/red). Amino acids that may interact with heme by hydrogen bonding with the propionate groups are shown in yellow. Trp156 (cyan) is also shown as it is positioned below the heme plane and was used as a spectroscopic handle (discussed later). Cys129 (green) is the only cysteine present in the cytosolic domain and is relevant to later discussion of intermolecular disulfide bond formation (PDB entry: 4X8Y).

In 2016, the X-ray crystal structure of the PGRMC1 cytosolic domain was published, showing that PGRMC1 binds heme (Figure 1, salmon).[12] In the crystal structure, heme binding appears to involve a single axial residue, Tyr113 (Figure 1, magenta), that directly coordinates to the heme iron to form a five-coordinate (5C) complex with an open axial coordination site.[7, 9, 12] In the same manuscript, Kabe et al. hypothesized that it is the heme-mediated PGRMC1 dimer that is required for the interaction with CYPs and EGFR,[12, 26] and that the PGRMC1 dimer is formed through hydrophobic heme (π-π) stacking. Support for the proposed heme-stacked dimer model

comes from an X-ray crystal structure, analyzed using the Protein Interfaces Surfaces and Assemblies (PISA) software.[26, 32]

Another potential route to form PGRMC1 dimers is through intermolecular disulfide bonding. Disulfide bonds are widely appreciated to stabilize protein structure; however they are often sensitive to and are disrupted by addition of thiol-containing reducing agents. In the cases of mouse PGRMC1 and the yeast homologue, Dap1, dithiothreitol (DTT)-resistant dimers and tetramers have been reported.[7] Kabe et al. also noted that the heme-mediated dimer they studied was not sensitive to DTT, suggesting to them that disulfide-bond formation was not the dominant source responsible for generating PGRMC1 dimers.[12] However, the influence of disulfide bond formation in the absence of heme was not investigated, thus leaving open the question of whether the only cysteine amino acid in the heme-binding domain of PGRMC1, Cys129 (Figure 1, green), could contribute to early, apo-protein dimerization. Thus, additional studies are required to define and understand the precise mechanism(s) and pathway(s) involved in the formation of PGRMC1 multimers.

In the initial study that reported the interaction of PGRMC1 with CYPs, the authors also highlighted Tyr113 as playing an important role in facilitating the formation of the heme-mediated dimer, and claimed this effect is independent of intermolecular disulfide bond formation.[12] However, in more recent work, it is proposed that interaction of PGRMC1 with CYPs does not necessarily require heme and that Tyr113 is not absolutely required for heme binding.[13, 14] McGuire et al. concluded that while Tyr113 may not be required for heme binding in PGRMC1, it is required for PGRMC1 binding to Ferrochelatase (FECH), the terminal enzyme in mitochondrial heme synthesis.[14] This latest report seems to relate to an earlier publication[33] where the authors suggested that PGRMC1 may serve as a heme chaperone or sensor that plays an

important role in delivering newly synthesized heme to apo-hemeproteins in various cellular locations.[7, 9, 13, 14, 21]

Together, these reports underscore the fact that, to understand the requirement of heme in PGRMC1 dimerization, we need to first understand the structural and functional effects of heme binding in PGRMC1. Additionally, the mechanism underlying heme-mediated versus disulfide bond-mediated dimerization, and the role of disulfide bond formation in heme dependent versus independent dimerization pathways, remain unclear. Understanding the interplay between Tyr113 and intermolecular disulfide formation in facilitating PGRMC1 dimerization has direct implications in future studies aimed at defining the interaction interface between PGRMC1 dimers and CYPs involved in drug metabolism.

The present work aims to address these knowledge gaps by utilizing a combination of spectroscopic and computational techniques to report on the structural and electronic properties associated with PGRMC1 heme binding and PGRMC1 dimerization in solution. In this work, our results support the findings of McGuire et al. that Tyr113 is not an absolute requirement for heme binding. The data presented here also challenges early reports that Tyr113 is necessary for PGRMC1 dimerization. Furthermore, our results support a mechanism for PGRMC1 dimer and higher-molecular-weight oligomer formation *in-vitro* that involves heme-binding and formation of intermolecular disulfide bonds. Interestingly, these pathways seem to act in concert in the wild-type protein but can be selectively highlighted using several site-directed variants, each of which displays their own unique oligomerization trends.

MATERIALS AND METHODS

Plasmid Construction. The codon optimized, cytosolic, heme binding domain of human PGRMC1 (amino acids 44-195 from UniProt entry O00264; Protein Data Bank (PDB) entry: 4X8Y), with a 6-His-tag, Tobacco Etch Virus (TEV) binding site and custom overhangs, was cloned into a pET28 vector with ampicillin resistance gene using the Gibson Assembly method. The complete, codon-optimized g-block for the cytosolic domain of PGRMC1 was ordered from Integrated DNA Technology (IDT). The plasmids used for Gibson Assembly are shown in Table S1. The pET28_His_TEV_PGRMC1 WT vector was transformed into NEB 5-alpha competent *Escherichia coli (E. coli)* cells (New England Biolabs), and mini preps were carried out to obtain purified plasmids that were then sent for Sanger sequencing (GENEWIZ LLC, Azenta Life Sciences). The verified sequence for WT PGRMC1 is shown below:

HHHHHHSSGENLYFQGSHKIVRGDQPAASGDSDDDEPPPLPRLKRRDFTPAELRRFDGV
QDPRILMAINGKVFDVTKGRKFYGPEGPYGVFAGRDASRGLATFCLDKEALKDEYDDL
SDLTAAQQETLSDWESQFTFKYHHVGKLLKEGEEPTVYSDEEEPKDESARKND

Y113F, C129S and Y113F/C129S (2X MUT) variants were prepared using a Q5-Quick Change Site-Directed Mutagenesis kit from New England Biolabs. Preparation of the 2X MUT was performed starting from the C129S PGRMC1 construct. Primers used for the mutagenesis are shown below in Table S1. All sequences were verified by Sanger sequencing.

Protein Expression. Aliquots of the transformation product were plated on LB agar + ampicillin plates and were grown in a stationary incubator at 37 ^{o}C overnight. Bacterial colonies of pET28_His_TEV_PGRMC1 NEB-5-alpha were inoculated into LB broth with 0.1 mg/mL Ampicillin (Quality Biological^{TM}) and were grown overnight in a 37 ^{o}C shaker incubator set to 220 rpm. The inoculated cultures were isolated, mini preps were made, and purified plasmids were sent to GENEWIZ LLC for Sanger sequencing. The sequence-verified, purified plasmid was then

transformed into BL21 (DE3) competent *E. Coli* cells (New England Biolabs) and inoculated following the same procedure. After 18 h, the culture was seeded into 0.5 to 4 L LB broth with 0.1 mg/mL Ampicillin and grown at 37 ºC (220 rpm) until the OD600 reached 0.5-0.6. Protein expression was induced by adding isopropyl β-D-1-thiogalactopyranoside (IPTG) to a final concentration of 1 mmol/L. The induced cultures were incubated overnight at 25 ºC with shaking at 100 rpm. Cultures were then centrifuged at 4 ºC and 4000g for 20 min. The cell pellet was then recovered and stored at -80 ºC until it was ready for lysis.

Protein Purification. Each 4 L scale-up yielded approximately 10 g of cell pellets. The cell pellets were resuspended in 100 mL of lysis buffer (50 mM sodium phosphate monobasic, 150 mM sodium chloride, 10 mM imidazole, 5% glycerol, 0.1% triton-X-100, pH7.5), with 2 units of Benzonase Nuclease (Novagen) per mL cell culture, 1 mM magnesium chloride and 1 mg/mL lysozyme (G-Biosciences). The cells were lysed by sonication (QSonica Sonicator, Model: Q55 with 1/8 in. probe) at 80% amplitude, for a total of 10 min (each cycle was 15 s on and 15 s off). Following sonication, the lysate was centrifuged at 35,000g at 4 °C for 1 h. The clarified supernatant was then filtered through a 0.45 μm sterile syringe filter, loaded onto a Ni-NTA affinity gravity flow column (G-Biosciences) and incubated for 1 h at 4 ºC, after which time the flow through was collected. The column was washed with 1 column volume (CV) wash buffer I (50 mM sodium phosphate monobasic, 100 mM sodium chloride, 20 mM imidazole, pH7.5) and 1 CV wash buffer II (50 mM sodium chloride, 50 mM sodium phosphate monobasic, 50 mM imidazole, pH7.5). The protein was eluted with 1.3 CV elution buffer (50 mM sodium phosphate monobasic, 150 mM sodium chloride, 250 mM imidazole, pH 7.5). Eluted protein was dialyzed into a buffer containing 150 mM sodium chloride, 50 mM sodium phosphate monobasic, 0.5 mM ethylenediamine tetraacetic acid (EDTA), pH 7.5 using 10k molecular weight cutoff (MWCO)

dialysis cassettes (Thermo Scientific™ Slide-A-Lyzer™ G2 Dialysis Cassettes). The His-tag on the protein was cleaved by TEV protease (protein to TEVp ratio 1:100) after 48 h incubation at 4 ºC. TEV protease is produced in-house from stocks prepared using the plasmid pDZ2087 (pDZ2087 was a gift from David Waugh; Addgene plasmid #92414; http://n2t.net/addgene:92414; RRID:Addgene_92414).[34] The His-tag cleaved protein was dialyzed against binding buffer containing 10 mM imidazole, and then loaded onto an equilibrated Ni-NTA gravity flow column. Protein run through the second column was collected in the flow-through (binding buffer) fractions as well as in the initial wash buffer. The purity of the protein fractions was assessed using 12% sodium dodecyl sulfate poly(acrylamide) gel electrophoresis (SDS-PAGE). Gels were stained with Bio-Safe Coomassie Blue (Bio-Rad). Protein samples were concentrated using 10,000 MWCO filters (Amicon) and dialyzed against buffer without imidazole. Protein concentrations were measured (A280, A260/A280) using a ThermoScientific NanoDrop One spectrometer, and the purified, concentrated protein samples were stored at 4 ºC in salt-phosphate buffer (150 mM sodium chloride, 50 mM 50 mM sodium phosphate monobasic, pH 7.0) for no longer than one month. For longer-term storage, PGRMC1 is stored in buffers containing 20% glycerol at -20 ºC.

The same protein purification protocol is followed for Y113F, C129S and Y113F/C129S (2XMUT) PGRMC1 mutants. The main difference was that TEV-digestion of the variants required a protein:TEV protease ratio of 1:80.

Heme-Protein Sample Preparation. One milliliter hemin solution was prepared by dissolving pre-weighed hemin powder (Chem Impex International Inc.), with 3 drops of 1 M NaOH, 1 mL of 150 mM sodium chloride, 50 mM sodium phosphate monobasic, pH 7.0 buffer. The solution was filtered to remove undissolved solid. A 1000-fold dilution was used to determine the concentration of the heme solution by UV/visible absorption spectroscopy (ε_{385nm} = 58,400 M^{-1} cm^{-1}). If needed,

the hemin solution was further diluted with the same buffer to achieve the desired final concentration. One milliliter of the hemin stock solution and 1 mL protein solution, prepared in the same buffer, were degassed on a Schlenk line equipped with Argon gas for ~30 min. All materials were then transferred into an anaerobic glovebox under Argon atmosphere. Before addition to apo-protein, a stoichiometric amount of DTT was added to the hemin solution. One molar equivalent (equiv) of heme stock solution was titrated into the protein, and samples were then incubated at 4 ºC in the dark for at least 1 h.

Circular Dichroism (CD) Spectroscopy. Thermal denaturation CD studies of heme-PGRMC1 samples (protein concentrations ~13 μM) were carried out with a focus on the far-UV region. Spectra were collected on an Applied Photophysics Chirascan V100 CD spectrometer equipped with a Xenon lamp and large area avalanche photodiode detector (LAAPD). Samples were loaded into 0.5 mm pathlength 6Q quartz cuvettes (Starna Cells), and data were collected from 190-250 nm with a step size of 1 nm at 10 ºC. All CD spectra were baseline corrected by subtracting the buffer spectrum. Thermal denaturation measurements were conducted across the temperature range from 10 to 84 °C, with the temperature ramped in 2 °C stepwise increments at a rate of 1 ºC/min using a Peltier temperature control unit and a recirculating water bath.

CD and absorption spectra in the UV-Visible region (300 to 700 nm) were collected for heme-PGRMC1 samples at concentrations of ~88 μM. These measurements were performed in a 2 mm pathlength 6Q quartz cuvette with airtight septum sealed cap.

Density Functional Theory (DFT) Calculations. Heme-bound WT (with Tyrosinate 113) and Y113F PGRMC1 monomer models were built starting from the x-ray crystal structure, PDB: 4X8Y.[12] These models include heme as well as the primary (Tyr113/Phe113) and secondary coordination sphere residues (Lys105, Phe106, Tyr107, Trp156, Lys163, Tyr164 and one

crystallographic water molecule). Amino acids were truncated at their C-α carbons, which were capped with methyl groups. One hydrogen atom from each methyl cap was frozen to mimic the constraints from the protein backbone. All geometry optimizations were carried out using Gaussian 09 revision e.01. The functional and basis sets used were B3LYP and LANL2DZ, including the pseudopotential for Fe and 6-31G* for C, N, H, and O atoms respectively. The self-consistent reaction field method was applied in all optimizations to account for solvation effects. In previously established protein models featuring tyrosine binding to heme to create a 5C complex, the tyrosine is typically in a deprotonated form.[35-43] Therefore, in the calculations for the wild-type (WT) PGRMC1 monomer, Tyr113 is assumed to be deprotonated, resulting in a total charge and multiplicity of 0 and 6, respectively. In the case of Y113F PGRMC1, the total charge and multiplicity remains 0 and 5, respectively. Visualization of the model was performed using GaussView 6.0.16.

Fluorescence Spectroscopy. The fluorescence emission spectra for apo-WT and Y113F PGRMC1 (~1 μM) were recorded in 6Q quartz cuvettes (Starna cells) with 1 cm pathlength at 5 ^{o}C using a Shimadzu RF-6000 spectrofluorometer equipped with TC1 temperature controller. The excitation wavelength was set at 295 nm and the emission spectra were recorded across the range from 310 to 500 nm. Titrations were performed by adding increasing amounts of heme to the WT/Y113F PGRMC1 samples. Binding constants were obtained by fitting the data to a nonlinear exponential decay using Origin 2022b (9.9.5.167 version).

Electron Paramagnetic Resonance (EPR) Spectroscopy. EPR samples of apo-WT PGRMC1, WT PGRMC1 with 1 and 2 equiv. of heme, and heme-only samples were prepared at concentrations of ~500 μM in 150 mM sodium chloride, 50 mM sodium phosphate monobasic, pH 7.0. Spectra were collected on a Bruker EMXplus X-band continuous wave (CW) EPR

spectrometer with a 9.5 in. double yoke magnet for studies ranging from room temperature to ~4.5 K. This setup includes high-sensitivity and dual-mode resonators for concentration limited or integer spin samples. Samples were measured in high-quality quartz EPR tubes (Wilmad-Labglass) using collection parameters 0-5000 G, 8 G modulation amplitude, 20 dB power attenuation, 4.5 K and 9.63 GHz, unless stated otherwise.

Size Exclusion Chromatography (SEC). SEC studies were performed using 250 μL of 10 μM heme-PGRMC1. Samples were loaded onto an ENrich SEC 70 high resolution size exclusion column (Bio-Rad) equilibrated with 150 mM sodium chloride, 50 mM sodium phosphate, pH 7.0 buffer. The NGC chromatography Bio-Rad NGC fast protein liquid chromatography (FPLC) system, version 3.3, was run at a rate of 1 mL/min, and the column was pre-equilibrated with the same running buffer before each run. The NGC system is equipped with a multi-wavelength detector to record the protein and heme (Soret band) absorbances simultaneously.

RESULTS

Establishing Spectral Benchmarks for Heme Binding to WT and Y113F PGRMC1. It is well known that heme moieties display intense Soret and slightly weaker Q-bands, and that the energies of these features shift in response to changes at the metal centers and substituents on the porphyrin ring.[44-48] By exploiting the sensitivity of these spectral features to molecular-level changes in the vicinity of the heme, we were able to detect heme binding to PGRMC1 using absorption and CD spectroscopy in the visible energy range. Figure 2A shows UV−vis spectra of WT PGRMC1 in the presence (blue) and absence (black) of equimolar heme, as well as for the heme-only control (red). The ferrous Fe(II) heme signal in the heme-only sample features a Soret band with an absorbance maximum at approximately 383 nm and Q-bands in the range of 550-580 nm. By

comparison, the Soret band of the anaerobically prepared WT PGRMC1-heme complex is observed at approximately 392 nm, with Q-bands in the range of 500-540 nm and a charge transfer band at 627 nm. The relatively high increase in the Soret band intensity, blue shift in the Q-bands, and observation of a new charge transfer band are consistent with the formation of a five-coordinate (5C) heme-bound PGRMC1 complex.[7, 8, 12]

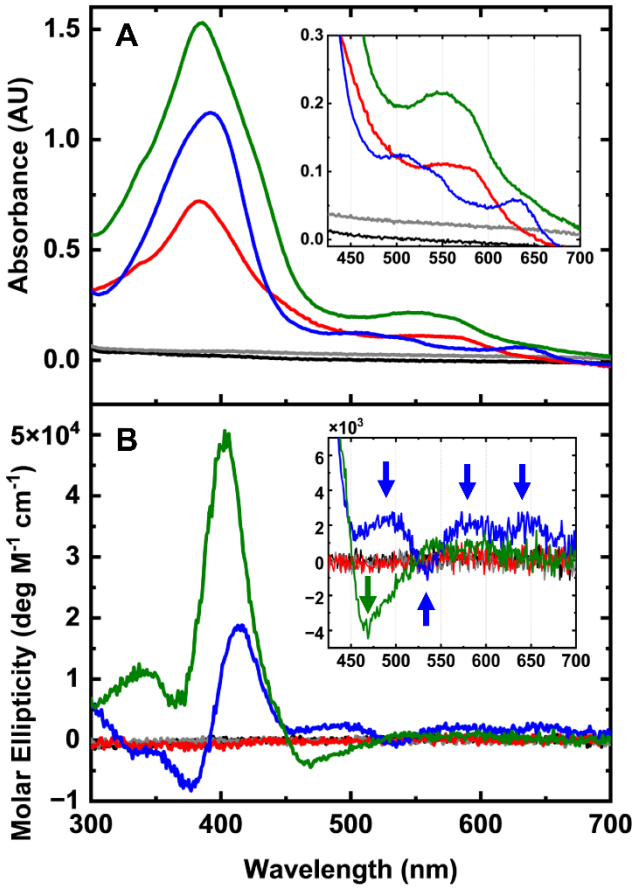

Figure 2. UV-vis absorption (A) and CD (B) of heme binding to WT PGRMC1 and Y113F PGRMC1. The spectra correspond to ~88 μM apo-WT PGRMC1 in chloride-phosphate buffer (black), ~88 μM apo-Y113F PGRMC1 (gray), equal concentration heme (only) sample (red), WT PGRMC1 with 1 equiv of heme (blue) and Y113F PGRMC1 with 2 equiv of heme (green). An explanation for why 2 equiv of heme were added to the Y113F variant is presented in the results section below. Figure insets show zoomed-in views of the weaker intensity absorbance and CD features in the region from 425 nm to 700 nm.

To gain further insight into the nature of heme binding to WT PGRMC1, we carried out CD studies in the visible energy region. Figure 2B shows that neither heme only nor apo-PGRMC1 exhibited any CD signals in the visible range (red and black spectra). However, when 1 equiv of heme is titrated into a solution containing WT PGRMC1, and the sample is incubated under anaerobic conditions, in the dark, for ~1 h at 4 °C, we measured the CD spectrum shown in Figure 2B (blue). This spectrum derives from protein-induced chirality[49, 50] and definitively confirms the formation of the heme-PGRMC1 complex. The blue spectrum in Figure 2B is comprised of approximately 8 peaks that derive from metal-ligand (MLCT) or ligand-metal (LMCT) charge transfers in the heme-coordinated PGRMC1 complex (Figure S1A). Furthermore, the fact that the CD intensity does not increase beyond the addition of one molar equiv of heme indicates that the protein heme-binding site is fully saturated at a heme:PGRMC1 stoichiometry of 1:1 (Figure S2A).

To evaluate the requirement for Tyr113 in heme binding to PGRMC1, we recorded visible CD data for the Y113F PGRMC1 variant in the presence of increasing concentrations of heme (1, 1.5 and 2 equiv). The results indicate that achieving saturation in Y113F PGRMC1 (Figure S2B) over similar incubation times as studied in WT PGRMC1, requires addition of 1.5-2 equiv of heme. This result suggests that the Y113F variant binds heme less tightly than the WT protein, owing to the mutation of the sole heme iron-binding residue. Perhaps not suprisingly, the spectrum of heme-bound Y113F PGRMC1 is distinct from that of heme-bound WT PGRMC1, and shows three distinct peaks at 335, 406, and 464 nm (Figures 2B, green and S1B).

In conclusion, the visible CD data for the WT and Y113F PGRMC1 samples, unequivocally confirms heme binding to PGRMC1, regardless of the presence of Tyr113. Moreover, in the presence of higher heme concentrations, Y113F PGRMC1 shows a unique

spectrum distinct from that of heme-bound WT PGRMC1, whereby highlighting differences in geometric and electronic structures of these two complexes.

Heme Binding to PGRMC1 Enhances the Thermal Stability of the Protein. CD spectroscopy was also employed to analyze the secondary structures of apo- and heme-bound WT PGRMC1. Experimental CD spectra are simulated using the online "CD fitter and simulator" software.[51] Our experimental data shows peaks for both apo- and heme-bound WT PGRMC1 that are characteristic of random coil (200 nm) and α-helix (208 and 222 nm) structural features. Simulation of the CD spectra revealed that both apo- and heme-bound WT PGRMC1 contain ~35% of α-helix, ~10% β-sheet, and ~55% random coil character (Figure S3). The relative percentages of each correlate well with calculated values obtained using the YASARA visualization software[52-54] to analyze the available crystal structure (PDB: 4X8Y).[12]

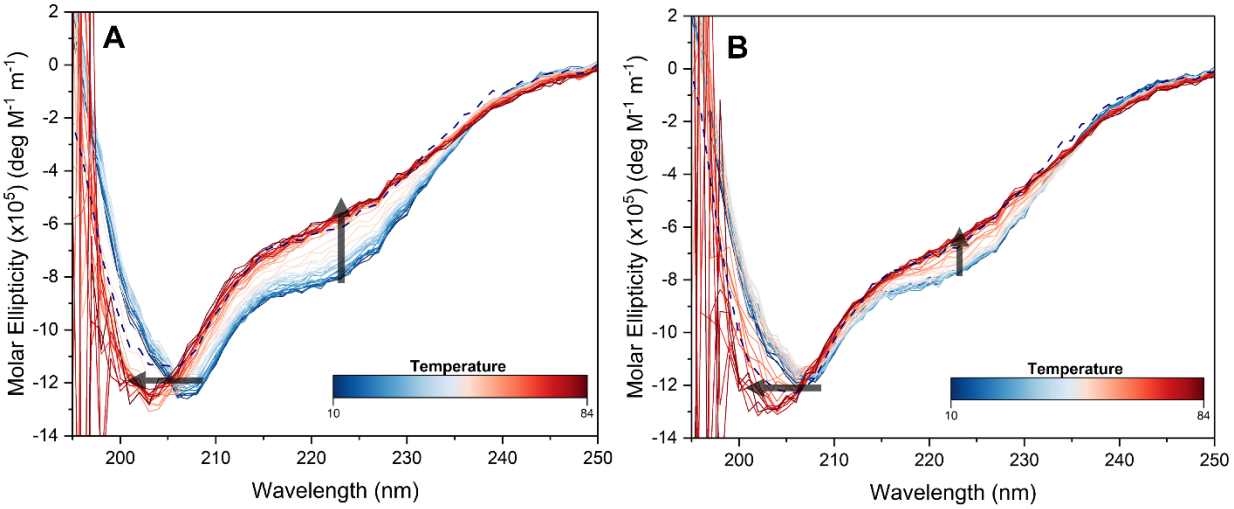

Figure 3. Thermal stability of (A) apo- and (B) heme-bound WT PGRMC1. CD thermal denaturation data are plotted for a variety of temperatures ranging from 10 to 84°C (increasing temperature from blue to red). Dashed curves represent the measurements recorded after thermal denaturation of the protein and return to a temperature of 10 °C.

We performed thermal denaturation studies to quantitatively assess protein stability and determine the melting temperature (T_m) of WT PGRMC1 in both the absence and presence of heme. In Figure 3A, as temperature increases (blue to red), we observe a decrease in the characteristic α-helix peak intensity at 222 nm for apo-WT PGRMC1 with a concomitant increase in random coil signal around 200-205 nm. The sigmoidal temperature versus CD intensity curves (Figure S5), in combination with analysis using the Global3 software from Applied Photophysics, enabled us to calculate a T_m value of approximately 50 °C for apo-WT PGRMC1 (Table 1). The CD data collected at 10 °C for PGRMC1 with 1 molar equiv of heme did not show significant spectral differences compared to the apoprotein in the far-UV region. However, the thermal denaturation data recorded for this sample (Figure 3B, blue to red) do show a decrease in the intensity of the α-helical signature. Using these data, we calculated a T_m of approximately 62 °C for the heme-loaded samples (Table 1). The notable difference in T_m values of 12 °C between apo- and heme-loaded WT PGRMC1 suggests that heme binding results in formation of a more stable complex. We propose that the increased stability is due to the fact that second sphere residues (Tyr107, Trp156, Tyr164, and Lys163) that appear to be important for stabilizing the heme in the binding pocket of WT PGRMC1 also reside in well-structured α-helices (Figure 1).

Table 1. Melting Temperature (T_m, °C) of PGRMC1 (WT, C129S, and Y113F) ± Heme.

PGRMC1	melting temperature (T_m) in °C	
	without heme	with 1 equiv of heme
WT	50.4	62.8
C129S	48.9	62.4
Y113F	50.9	56.0

Although we have focused up to this point on Tyr113, and have only briefly mentioned Cys129 in the introduction, it is important to acknowledge that, in the absence of heme, Cys129 may also play a role in promoting adventitious dimerization. The role of Cys129 in facilitating

dimerization will be discussed further in the following sections; however initial characterization is presented here to establish the model. Thermal denaturation data were also collected for Y113F and C129S variants (Figure S4). Both Y113F and C129S PGRMC1 displayed similar spectral changes to those of the WT protein upon increasing temperature. The calculated T_m for apo-Y113F is approximately the same as that of WT protein. However, analysis of the data for apo-C129S revealed a T_m of approximately 49 ^oC, suggesting that formation of a putative disulfide bond, even in the absence of heme, could confer additional stabilizing benefits to PGRMC1 (Figure S5 and Table 1). Upon heme addition to apo-Y113F PGRMC1, we observed a modest increase in T_m of 6 ^oC. Considered in isolation, the thermal denaturation data collected for WT and C129S PGRMC1 provide compelling evidence in support of the role of Tyr113 in heme binding and subsequent protein stabilization (Figure S5 and Table 1).

Energy Optimized Models of Heme Binding to WT and Y113F PGRMC1. To further define the effect of heme-binding on the structure of PGRMC1, we performed DFT calculations using the model described herein (Materials and Methods, Figure 4). Our DFT calculations confirm that Tyr113 binds to the heme iron in WT PGRMC1 as tyrosinate, to form a 5C complex. Energy optimization of an *in silico* generated Tyr113 to phenylalanine (Y113F) variant revealed that the Phe113-heme iron distance (~2.73 Å) is significantly longer than the Tyr113-heme iron distance (~1.98 Å) in WT PGRMC1 (Tables S4 and S5). Furthermore, in Y113F PGRMC1, the heme remains four-coordinate with two open axial positions (Figure 4C,D). This result is consistent with a previous report and suggests that although there is no direct bonding interaction between the heme iron and the protein, residues in the binding pocket play a critical role in stabilizing heme via the propionate groups (Figure S6).[12]

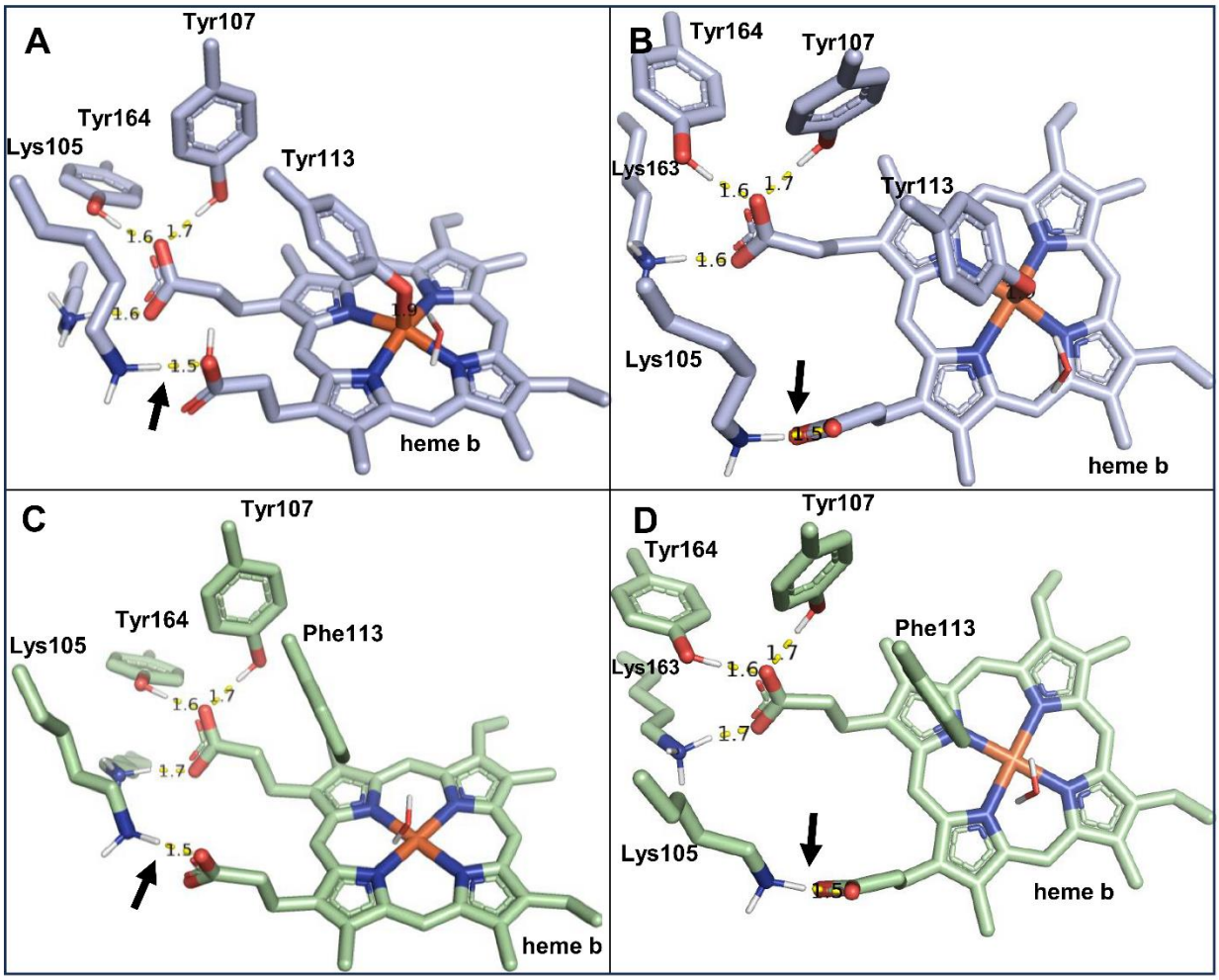

Figure 4. DFT geometry optimized models of the heme-binding domain of (A,B) WT PGRMC1 (slate blue) and (C,D) Y113F PGRMC1 (green). Hydrogen bonding interactions are indicated by yellow dashed lines. In parts (A) and (C), Lys163 and Tyr164 are partially obscured. The previously unmentioned residue Lys105 that participates in a H-bonding interaction with one of the heme propionate groups is indicated by the black arrow. All H-bonding distances shown are in units of Å. Detailed bond length information for WT and Y113F PGRMC1 is provided in Tables S4 and S5. Although mentioned elsewhere, Phe106 and Trp156 have been omitted for clarity.

To gain insight into heme binding in the absence of Tyr113, we revisited previous works[12, 13] highlighting Tyr107, Lys163 and Tyr164 (Figure 1, yellow) as being important for stabilizing the heme moiety in the binding pocket of PGRMC1. This hypothesis is supported by the DFT calculations presented here. The bond lengths and interatomic distances between key residues before and after optimization are listed in Table S4. As expected, in WT and Y113F models, both

heme propionate groups seem to be in close proximity to Lys163 and Tyr164, which supports the earlier studies that Lys163 and Tyr164 could stabilize heme binding to PGRMC1 (Table S5).[12] Interestingly, the previously unmentioned residue Lys105 also appears to play an important role in stabilizing the heme propionate groups in the binding pocket (Figure 4, indicated by the black arrow) in both WT and Y113F. These observations support the hypothesis that, apart from axial Tyr113, H-bonding interactions with Lys105, Tyr107, Lys163, and Tyr164 could be sufficient to stabilize the propionate groups of heme, thereby stabilizing the heme-PGRMC1 complex.

Intrinsic Tryptophan (Trp) Fluorescence as a Probe to Identify the Heme Binding Site in PGRMC1. The location of heme binding in PGRMC1 was demonstrated using fluorescence spectroscopy. Utilizing the intrinsic Trp fluorescence and the fact that there is only one Trp in our PGRMC1 system (Trp156) (Figure 1, cyan), we were able to monitor changes in the local Trp environment in response to heme addition.[55] Upon excitation at λ_{ex} = 295 nm, Trp in water at neutral pH gives rise to a spectral feature with emission maximum at 348 nm.[56] In the case of our protein system, we expect that structural changes in the vicinity of Trp156 that are caused by heme interactions, protein conformational changes, self-association, or protein folding/denaturation would alter both the fluorescence intensity as well as the emission wavelength.[7, 56-58]

To determine whether the heme does indeed interact with PGRMC1 in the vicinity of Trp156, we recorded spectra for apo-WT PGRMC1 in the absence and presence of increasing concentrations of heme. Data were recorded using λ_{ex} = 295 nm, and the fluorescence spectra were measured over the range from 310 to 500 nm (Figure 5). Apo-WT PGRMC1 yields a strong fluorescence signal with a maximum at 333 nm (Figure 5, black), attributable to Trp156 that is positioned near the heme binding pocket (Figure 1). The addition of 0.2 to 10.4 molar equiv of

heme to PGRMC1 resulted in quenching of the fluorescence signal (Figure 5), indicating that the local environment around the tryptophan has changed relative to the apoprotein. Importantly, this quenching behavior saturates after addition of 1 molar equiv of heme. Thus, we conclude that addition of heme results in a less solvent-exposed, more buried Trp156, which is consistent with heme binding in the vicinity of Trp156. This interpretation is further supported by the slight blue shift in the fluorescence feature from 333 to 330 nm, which suggests the environment around Trp156 becomes more hydrophobic.

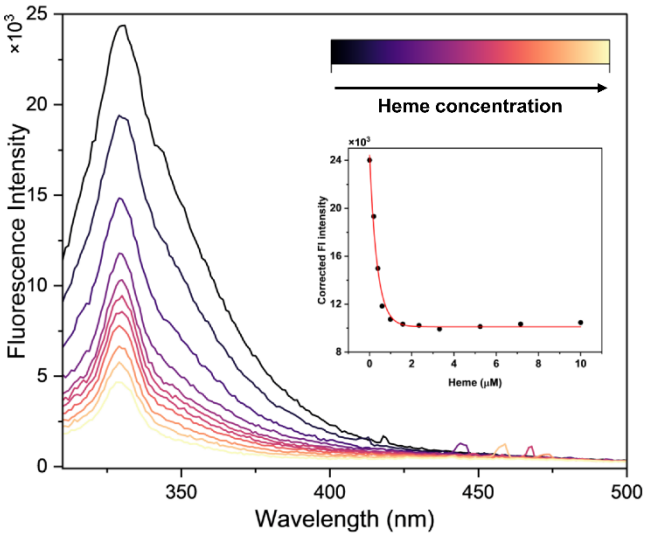

Figure 5. Raw intrinsic Trp fluorescence spectra of heme binding to apo-WT PGRMC1 (1 μM) (black) with increasing concentration of heme (from 0.2 equiv to 10 equiv), λ_{ex} = 295 nm. Inset: titration curve of WT PGRMC1 with heme. The data were fit using the equation y = 14307.47*exp(-x/0.36) +10107.14 to obtain a K_d value of 2.77 ± 0.23 μM.

We carried out the same study for the Y113F variant and observed similar fluorescence quenching with increasing heme concentrations (0.2 to 10.4 equiv) (Figure S7). After subtracting the spectral contribution from the inner filter effect of heme,[59] we obtained K_d values of 2.77 ± 0.23 μM and 1.71 ± 0.096 μM for WT and Y113F PGRMC1 bound heme, respectively (Figures 5 and S7). Although these K_d values are of a similar order of magnitude to those reported by McGuire

et. al, they are distinct from each other, suggesting there is a difference in heme binding with/without Tyr113.[13]

Defining the Electronic and Geometric Structures of the PGRMC1 Monomer and Dimer Using EPR Spectroscopy. Low temperature EPR spectra of WT PGRMC1 in the presence of 1 equiv (black) and 2 equiv (red) of heme are shown in Figure 6. These spectra feature distinct peaks with *g*-values ~6 and ~1.99 that resemble those previously reported for axial 5C high-spin (HS) Fe(III) species,[7, 36, 38, 39, 60-64] thus allowing assignment of the heme iron oxidation state (Figure S8). As shown in Figure 6 (blue), addition of 0.5 equiv heme to the C129S PGRMC1 variant yields an EPR signal that resembles that of WT PGRMC1 in the presence of 1 equiv heme, with a weak, low field shoulder observed in the C129S spectrum. In summary, the EPR spectra recorded for heme-bound WT and C129S PGRMC1 are characteristic of a high spin heme in an axial zero field splitting environment.

Comparison of the EPR data for WT PGRMC1 with 1 versus 2 equiv of heme reveals a slight decrease in the EPR signal intensity with increasing heme concentration. This subtle decrease in the EPR signal intensity, most clearly seen in the derivative feature near $g \sim 6$ may suggest slower formation of an antiferromagnetically coupled WT PGRMC1 dimer wherein the two heme molecules are close enough to experience a through space interaction with one another.

Interestingly, no perpendicular mode EPR signals were observed for Y113F and C129S PGRMC1 variants with 1 and 2 equiv heme, suggesting that the heme site in these systems is distinct from that of the wild-type protein. The most obvious reason for this, in the case of the Y113F variant, is that in the absence of Tyr113, there is no direct interaction between the protein and the heme iron, thus allowing for the iron to remain as an S=2 integer spin Fe(II) species that is EPR silent in perpendicular mode. In the case of the C129S variant with 1 or 2 equiv of heme,

one potential reason for a lack of EPR-detectable signal may be that, in the absence of Cys129 the PGRMC1 monomers are able to orient themselves more effectively for productive interaction and stacking between the two heme moieties to yield an antiferromagnetically coupled heme-mediated dimer. However, additional studies are necessary to understand the electronic structure of the PGRMC1 dimer model fully.

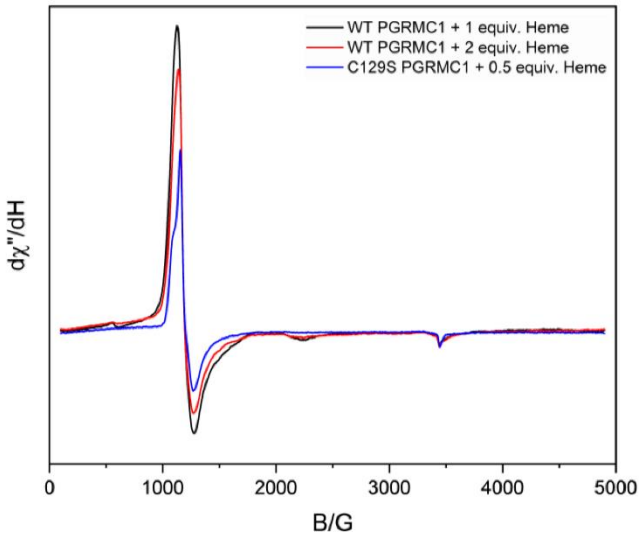

Figure 6. Overlay of EPR spectra of WT PGRMC1 with 1 (black) and 2 (red) equiv of heme, and C129S with 0.5 equiv of heme (blue). EPR measurement parameters: 8 G modulation amplitude, 20 dB, 9.63 GHz, and 4.5 K.

Detection of the PGRMC1 Dimer in the Presence and Absence of Heme. To further monitor the influence of heme addition on PGRMC1 monomer/dimer speciation, we turned to SDS-PAGE and SEC. SDS-PAGE data of dimerization in WT as well as C129S and Y113F mutants (Figure S9) was collected; however this technique has the inherent limitation that it does not readily resolve the multitude of interactions we are interested in characterizing.[65] Thus, to further explain our EPR findings and explore potential routes for PGRMC1 dimerization, we utilized SEC. Using a multiwavelength UV-Vis detector in line with a Bio-Rad NGC FPLC system and a SEC70 column (Bio-Rad), we monitored the absorbance at 280 nm (A280). SEC studies of WT PGRMC1 and

mutants (C129S, Y113F, Y113F/C129S also referred to as 2XMUT) were carried out in the absence and presence of heme (0.5, 1, 2, 3 molar equiv of heme). The resulting chromatograms are shown in Figures 7 and S10. The chromatogram for apo-WT PGRMC1 (Figures 7A, green and S10A) shows two peaks that eluted around 10 and 11 min after loading. Based on calibrations using known protein standards, these peaks correspond to apo-PGRMC1 in the dimeric and monomeric conformations, respectively. The presence of the dimer conformation, even in the absence of heme, likely results from an intermolecular disulfide bond between Cys129 residues in adjacent PGRMC1 monomers (Figures 7A, green and S10A).[12] Data collected after addition of 0.5-1 equiv of heme (Figure 7B,C) clearly show a shift in population from predominantly monomer species to predominantly dimer. By evaluating the area under each curve, we estimate that the percent speciation of WT PGRMC1 species changes from 49% monomer/ 41% dimer to 16% monomer/75% dimer in apo- and 1 equiv heme-loaded samples, respectively (Figure S11A,E). Incubation with higher heme concentrations (2-3 equiv) resulted in the observation of a new peak that eluted 9 min after loading onto the column, and that likely corresponds to a higher molecular weight multimer (possibly a trimer or tetramer). In sum, the results from our SEC study of WT PGRMC1 suggest that (i) the formation of higher molecular weight/larger oligomers depends, at least in part, on heme concentration, and (ii) that PGRMC1 can exist as a dimer even in the absence of heme.

To confirm the degree to which dimerization requires formation of disulfide-bonds or heme binding, we utilized our C129S, Y113F, and 2XMUT PGRMC1 variants. SEC data recorded for the C129S mutant (Figures 7A, red and S10B**)** in which we have removed the potential for disulfide bond formation shows a single peak that eluted around 11 min after loading, suggesting little to no dimer formation. This result suggests that a dominant pathway for heme-independent dimerization

involves the formation of disulfide bonds between adjacent Cys129. Addition of 0.5-1 equiv of heme resulted in the observation of an elution peak at the position expected for the PGRMC1 dimer ($t_{elution}$ = 10 min), that increased at higher heme concentrations (2-3 equiv). This work confirms the existence of a heme-mediated dimerization pathway that operates independently of disulfide bond formation. Our findings also indicate there is a second, alternative route that operates independent of heme, and that requires Cys129.

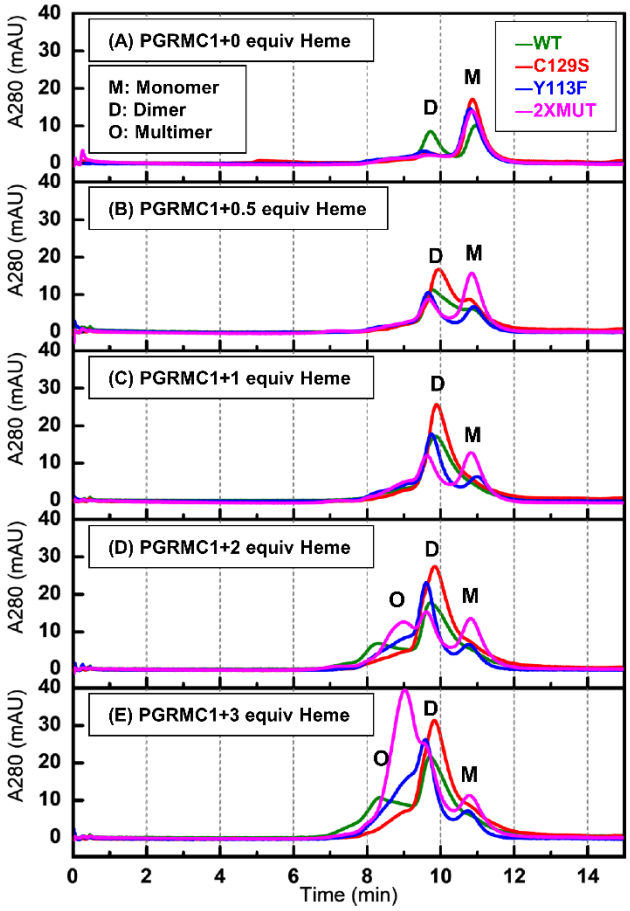

Figure 7. SEC run of WT, C129S, Y113F, and 2XMUT PGRMC1 in the presence of increasing heme concentrations. Absorbance traces at 280 nm are shown for the elution of PGRMC1. PGRMC1 concentrations were kept constant, whereas increasing concentration of heme is listed at the top of each plot.

To test if Tyr113 is essential for heme-mediated dimerization, we carried out parallel SEC

studies for Y113F and 2XMUT PGRMC1. The Y113F PGRMC1 data resemble those collected for the C129S variant, with the notable exception of the appearance of a more intense, larger species at highest heme concentrations (Figures 7, blue and S10C). This observation challenges previous hypotheses asserting the absolute necessity of Tyr113 for PGRMC1 dimerization. It is important to note that at the highest heme concentrations studied, we do not observe distinct peaks for trimer, tetramer, or larger protein multimers in the C129S and Y113F mutants. We do, however, observe broad shoulders left of the peaks corresponding to the dimer fractions. Interestingly, for our 2XMUT in the presence of 2-3 equiv of heme, we observed a very high intensity multimer peak and a shoulder at the position most consistent with the dimer (Figures 7, magenta and S10D).

DISCUSSION

Previous studies have shown that heme binds to PGRMC1 via a combination of direct coordination by Tyr113 and second-sphere residues that stabilize the propionate groups of heme b in the PGRMC1 binding pocket, and that these interactions may play important roles in heme-mediated homodimer formation.[7, 9, 12] However, recent work has called into question the requirement of Tyr113 for heme binding and downstream dimer formation.[13] The work presented here provides a definitive structural and electronic picture of heme binding in the cytosolic heme b binding domain of WT PGRMC1 as well as Y113F and C129S variants, and confirms the role of Tyr113 in heme binding as well as the degree to which it is required for PGRMC1 homodimer formation. These findings lay the foundation for us to define the molecular-level factors that influence the interaction of apo-/heme-loaded-PGRMC1 with CYPs responsible for metabolizing chemotherapeutic agents.

PGRMC1 Binds Heme in a Solvent Exposed Site, Irrespective of Tyr113. CD studies in the visible range and X-band EPR spectra for WT PGRMC1 provide conclusive evidence for heme binding to WT PGRMC1. The spectra are characteristic of a 5C HS Fe(III) site, closely resembling other heme systems that have been previously studied.[7, 36-39] Heme complexes with WT and Y113F PGRMC1 yielded distinct CD spectra in the visible energy region, suggesting non-trivial differences in the coordination environments and supporting the idea that there are multiple heme binding modes. EPR measurements recorded for the Y113F: heme complex do not show any EPR-active signals. This could be the result of removal of the only axial ligand to the heme iron in Y113F PGRMC1, thus allowing the heme iron to remain in its HS Fe(II), EPR-silent form. However, intrinsic tryptophan fluorescence measurements exploiting Trp156 in WT/Y113F PGRMC1 displayed similar trends for both samples. The measurable impact to the local environment and solvent accessibility at Trp156 indicates that heme binds both WT and Y113F PGRMC1 in its vicinity. The K_d values calculated here for WT and Y113F are comparable to those in previous reports.[13] However, our data paints a different picture of heme binding in Y113F PGRMC1, wherein the heme binding pocket, comprised of Lys105, Tyr107, Lys163 and Tyr164, stabilizes the heme via weak H-bonding interactions with its propionate groups (Figures 4 and S6). Although several of these residues have been identified before,[9, 12-14] this is the first report we are aware of that highlights Lys105. This picture is further supported by our thermal denaturation CD studies and DFT calculations for the WT and Y113F PGRMC1 samples. Most notably, addition of heme to apoprotein enhances protein stability, with calculated increases in T_m of 12 and 6 ^oC for heme-bound WT and Y113F PGRMC1, respectively. Finally, comparison of DFT energy optimized structures for WT and Y113F PGRMC1 reveals that in the absence of the tyrosinate moiety, the Phe variant cannot directly bind to the heme iron. Consequently, the heme iron remains

HS Fe(II), thereby precluding detection by perpendicular mode X-band EPR. Another important result from the present work is the observation that the WT and Y113F models appear to stabilize heme binding via H-bonding interactions with Tyr107 and Lys105. Additionally, our results support the earlier conclusion that while Tyr113 clearly plays a role in stabilizing heme binding to PGRMC1, it is not absolutely required.[12, 13] Broader implications of these results relate to early literature on PGRMC1 that identified Tyr113 as lying within a tyrosine kinase binding domain.[11] The thinking was that Tyr113 would be susceptible to phosphorylation, thereby providing a regulatory switch that would preclude heme binding and would impact subsequent membrane trafficking of full length PGRMC1.[11, 12, 66] Although it was hypothesized that heme-binding and phosphorylation of Tyr113 are mutually exclusive functions,[11, 12] our studies suggest that PGRMC1 retains its ability to form homodimers even in the absence (or phosphorylation) of Tyr113.

PGRMC1 Dimerization Proceeds via Several Routes. Early support for the heme-dependent PGRMC1 homodimer structure was provided by X-ray crystallography and PISA analysis.[12, 32] However, the data presented here indicate that adventitious dimerization of the cytosolic PGRMC1 domain appears to be, at least in part, heme independent. Although previous reports focused solely on the heme-heme stacking interaction as the main driver of protein dimerization, this work further explores the role of Cys129 in the heme-independent pathway. Not only was the WT PGRMC1 dimer sensitive to addition of thiol-containing reducing agents such as DTT or beta-mercaptoethanol (BME) (Figure S9), but SDS-PAGE and size exclusion chromatography of our C129S variant revealed majority monomer speciation in the absence of heme (Figures 7, red, S9C, and S10B).

Titration of 0.5 to 3 molar equiv heme resulted in a shift in speciation from monomer to dimer and ultimately larger oligomeric conformers, as detected via SEC. Quantitative analysis of the SEC chromatograms for PGRMC1 samples containing 1 equiv of heme revealed an increase in the dimer population compared to monomer. Both WT and the C129S variant displayed a similar distribution of monomer and dimer species, confirming a heme-dependent contribution to dimer and multimer formation (Figure S11E,F). As the heme concentration is further increased from 1 to 3 equiv WT and C129S PGRMC1 samples appear to be comprised of a majority dimer species, with some amount of higher molecular weight multimers (likely trimer and tetramer), and traces of the monomer population (Figures 7 and S10A,B). Conversely, in the case of Y113F and 2XMUT variants, even with increased heme concentrations up to 3 equiv, there is a nontrivial contribution to the SEC chromatogram from the monomer population (Figures 7 and S10C,D). This observation underscores the fact that although heme can still interact with the protein via its propionate groups, its binding efficiency and ability to form heme-mediated dimers is impacted by mutation of Tyr113.

These observations also indicate that there is a small contribution from the heme-dependent oligomerization pathway in all constructs (WT/Y113F/C129S/2XMUT) studied in the presence of 2 or more equiv of heme. Although we currently lack the resolution required to definitely assign the larger species as PGRMC1 trimers or tetramers, the fact that the elution peak is observed 9 min after sample loading clearly indicates that it is larger than the dimer (Figures 7 and S10). Interestingly, this higher molecular weight band is most intense in 2XMUT PGRMC1 with 3 molar equiv of heme. One possible explanation for this could be that in the absence of Tyr113 and Cys129, the heme is not locked into a specific orientation by direct coordination with the protein, thus allowing formation of a putative stacked heme trimer/tetramer chain. With the help of the

ClusPro docking tool[63, 67-69] we generated models for PGRMC1 trimers as well as tetramers. In each case, there seems to be a preference for stacking of heme molecules and alignment of alpha helices between adjacent protein molecules, whereby resulting in partially stable, larger oligomeric conformations (Figure S12). Given that this work focuses only on the cytosolic domain of PGRMC1, it is important to note that, even though we observed larger multimer formation in PGRMC1 at the highest concentrations of heme, such multimers are likely not physiologically relevant. Nevertheless, the observation of larger multimers does appear to be heme concentration dependent. This observation is particularly relevant when considered within the context of physiological stress which can result in excess production of heme.[70, 71] Under these conditions, the current work suggests that PGRMC1 would predominantly exist in a dimeric state. Thus, if the PGRMC1 dimer is indeed required for downstream PPIs, such conditions would likely facilitate interactions with cytochrome P450s.

Interestingly, low temperature X-band EPR data collected for each of these systems (WT, C129S, and Y113F) in the presence of 1 equiv of heme revealed additional differences in their electronic structure descriptions. Notably, WT PGRMC1 incubated with heme is expected to be primarily in the dimeric form by SEC, with the presence of PGRMC1 monomer species still evident, as judged by the shoulder in the SEC chromatogram. Despite this, X-band EPR still shows a signal characteristic of a HS Fe(III) heme. Granted, the two heme iron centers are estimated to be ~7.3 Å apart,[12, 26] as evaluated in the available crystal structure, thus potentially precluding direct coupling of the two spin centers which could result in a diamagnetic system to yield an EPR silent complex. This observation may be attributed to the potential presence of adventitious dimers, formed through intermolecular disulfide bonds alongside the heme-mediated PGRMC1 dimer. This discussion is particularly relevant given that EPR spectra of C129S PGRMC1 are

characteristic of a HS Fe(III) heme system when 0.5 equiv of heme is added and that at this heme concentration, SEC would predict that the majority of the protein is in the monomeric form. However, upon addition of increasing concentrations of heme (1-2 equiv), the C129S variant did not yield an EPR-active signal. In the case of Y113F, we established that the protein does not directly coordinate to the protein via the iron center. Thus, the heme iron would remain in its Fe(II) state even after incubation with PGRMC1, rendering the non-Kramers spin system silent in perpendicular mode X-band EPR. In the case of C129S, however, the protein is still able to coordinate to the heme iron via Tyr113 whereby the HS Fe(II) center is converted to HS Fe(III). One potential hypothesis for the lack of observable EPR signal in the C129S variant is that mutation of Cys129 removes steric/conformational restrictions that prevent the heme iron centers from moving closer to one another in the final dimer structure. If this hypothesis is correct, one could imagine that the two heme moieties may be able to move closer to one another (shorter Fe-Fe distance), leading to more effective antiferromagnetic coupling. This hypothesis suggests that the heme-mediated PGRMC1 dimer could show structural conformational differences as compared to the PGRMC1 dimer that results from disulfide bond formation.

Taken together, our work to define the roles of heme, Tyr113, and Cys129 in PGRMC1 homodimer formation seems to support a picture of PGRMC1 dimerization, whereby disulfide bond formation and heme-heme stacking act together to influence the overall structural and electronic description of the system (Figure 8). This unified perspective is also supported by the observation of broadened SEC peaks and the appearance of additional peaks corresponding to larger oligomeric species at the highest heme concentrations measured.

In summary, the present work confirms that PGRMC1 dimerization proceeds via two nonmutually exclusive routes that involve: (i) formation of intermolecular disulfide bonds and (ii)

hydrophobic heme (π-π) stacking. Previous *in-vivo* studies reported that PGRMC1 must form the heme-dependent dimer in order to bind/interact with CYPs.[12] This could mean that (i) the heme-mediated PGRMC1 dimer undergoes a structural/conformational rearrangement that distinguishes it from the PGRMC1 dimer arising from intermolecular disulfide bond formation, or (ii) heme itself may play a key role in the interaction of the PGRMC1 dimer and CYPs.

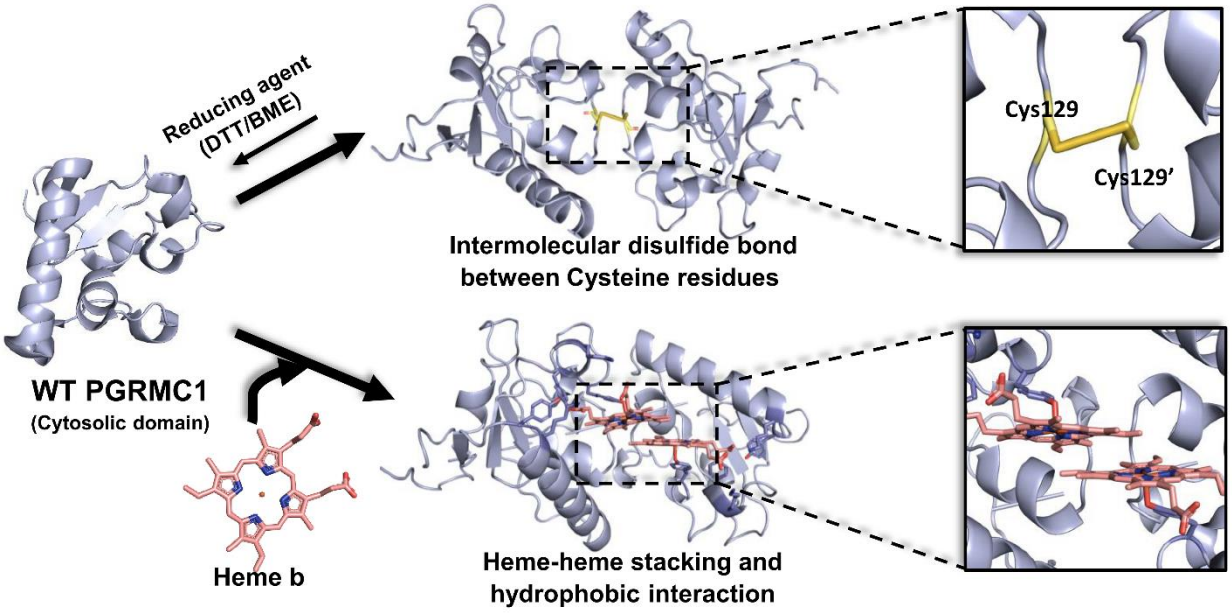

Figure 8. Possible pathways for PGRMC1 dimerization: (1) *(top)* Formation of an intermolecular disulfide bond between two cysteines (Cys129). This dimerization is reversible, transitioning back to a monomeric state in the presence of reducing agents like DTT and BME, and is independent of heme-binding. (2) *(bottom)* Dimerization through stacking of heme molecules. This process is not strictly dependent on the presence of Tyr113 and Cys129.

Implications for Future Studies.

The present work provides a clear description of heme binding to PGRMC1 and the roles of heme, Tyr113, and Cys129 in PGRMC1 dimerization. The structural and electronic characterization of heme-bound PGRMC1 presented here lays the groundwork for ongoing studies in our lab to characterize full-length PGRMC1 and its interaction with biomimetic membranes which would, presumably limit the explorable surface area for homodimer formation and

downstream interaction with CYPs. Moving forward, consideration of membrane bound full-length PGRMC1 will provide a better understanding of the physiological and functional relevance of the PGRMC1 dimer and multimers reported here.

ASSOCIATED CONTENT

Supporting Information

The Supporting Information is available free of charge.

Data in the Supporting Information file includes additional CD, Fluorescence, EPR spectra, SEC data, multimer models, and tables as mentioned in the text (PDF).

Accession Codes

This manuscript describes expression, purification, and spectroscopic characterization of UniProt entry O00264 (amino acids 44-195).

AUTHOR INFORMATION

*Corresponding Author

Katlyn K. Meier −Department of Chemistry, University of Miami, Coral Gables, FL, 33146, United States; orcid.org/0000-0002-8316-9199; Phone: 305-284-9807; Email: kmeier@miami.edu

Author

Prajakta Badve −Department of Chemistry, University of Miami, Coral Gables, FL, 33146, United States; orcid.org/0009-0009-9733-2733

Author Contributions

The manuscript was written through contributions of all authors. All authors have given approval to the final version of the manuscript.

Funding Sources

This work was supported by the National Science Foundation CAREER Award CHE-2144239 to K. K. M.

CONFLICTS OF INTEREST

There are no conflicts of interest to declare.

ACKNOWLEDGMENT

The authors declare no competing financial interests. This material is based upon work supported by the National Science Foundation CAREER Award CHE-2144239 to K. K. M. The authors greatly appreciate access to computational resources provided by the University of Miami Institute for Data Science and Computing (IDSC). The authors also acknowledge Allison Kelley (former undergraduate student) for carrying out the initial transformation, inoculation, scale-up and protein purification of Y113F PGRMC1.

ABBREVIATIONS

PGRMC1, Progesterone receptor membrane component 1; CYP, cytochrome P450; EGFR, epidermal growth factor receptor; MAPR, membrane-associated progesterone receptor; WT, wild-type; CD, circular dichroism; PPI, protein-protein interaction; PISA, Protein Interfaces Surfaces and Assemblies; FECH, Ferrochelatase; IPTG, Isopropyl ß-D-1-thiogalactopyranoside; Ni-NTA, nickel-nitrilotriacetic acid; CV, column volume; TEV, Tobacco Etch Virus; DTT, Dithiothreitol;

MWCO, molecular weight cut-off; LAAPD, large area avalanche photodiode; DFT, Density functional theory; EPR, Electron paramagnetic resonance; CW, continuous Wave; SEC, Size exclusion chromatography; FPLC, Fast protein liquid chromatography; MLCT, Metal-ligand charge transfer; LMCT, Ligand-metal charge transfer; 5C, five-coordinate; HS, High spin; Dap1, damage associated response protein 1; SDS-PAGE, Sodium Dodecyl Sulphate-Polyacrylamide Gel Electrophoresis; BME, beta-mercaptoethanol.

REFERENCES

1. Cahill, M. A., Progesterone receptor membrane component 1: an integrative review. *The Journal of steroid biochemistry and molecular biology* **2007,** *105* (1-5), 16-36.
2. Kimura, I.; Nakayama, Y.; Konishi, M.; Terasawa, K.; Ohta, M.; Itoh, N.; Fujimoto, M., Functions of MAPR (membrane-associated progesterone receptor) family members as heme/steroid-binding proteins. *Current Protein and Peptide Science* **2012,** *13* (7), 687-696.
3. Cahill, M. A.; Medlock, A. E., Thoughts on interactions between PGRMC1 and diverse attested and potential hydrophobic ligands. *The Journal of steroid biochemistry and molecular biology* **2017,** *171*, 11-33.
4. Mifsud, W.; Bateman, A., Membrane-bound progesterone receptors contain a cytochrome b5-like ligand-binding domain. *Genome biology* **2002,** *3* (12), 1-5.
5. Ohta, H.; Itoh, N., The membrane-associated progesterone receptor (MAPR) protein family. *Curr. Top. Biochem. Res* **2012,** *14*, 11-16.
6. Min, L.; Takemori, H.; Nonaka, Y.; Katoh, Y.; Doi, J.; Horike, N.; Osamu, H.; Raza, F. S.; Vinson, G. P.; Okamoto, M., Characterization of the adrenal-specific antigen IZA (inner zone antigen) and its role in the steroidogenesis. *Molecular and cellular endocrinology* **2004,** *215* (1-2), 143-148.
7. Ghosh, K.; Thompson, A. M.; Goldbeck, R. A.; Shi, X.; Whitman, S.; Oh, E.; Zhiwu, Z.; Vulpe, C.; Holman, T. R. Spectroscopic and Biochemical Characterization of Heme Binding to Yeast Dap1p and Mouse PGRMC1p. *Biochemistry* **2005,** *44* (50), 16729–16736.
8. Min, L.; Strushkevich, N. V.; Harnastai, I. N.; Iwamoto, H.; Gilep, A. A.; Takemori, H.; Usanov, S. A.; Nonaka, Y.; Hori, H.; Vinson, G. P., Molecular identification of adrenal inner zone antigen as a heme-binding protein. *The FEBS journal* **2005,** *272* (22), 5832-5843.
9. Kaluka, D.; Batabyal, D.; Chiang, B.-Y.; Poulos, T. L.; Yeh, S.-R. Spectroscopic and Mutagenesis Studies of Human PGRMC1. *Biochemistry* **2015,** *54*, 1638−1647.
10. Cahill, M. A.; Jazayeri, J. A.; Catalano, S. M.; Toyokuni, S.; Kovacevic, Z.; Richardson, D. R. The emerging role of progesterone receptor membrane component 1 (PGRMC1) in cancer biology. *Biochimica et Biophysica Acta (BBA)-Reviews on Cancer* **2016,** *1866* (2), 339-349.
11. Cahill, M. A.; Jazayeri, J. A.; Kovacevic, Z.; Richardson, D. R. PGRMC1 regulation by phosphorylation: potential new insights in controlling biological activity! *Oncotarget* **2016,** *7* (32), 50822.
12. Kabe, Y.; Nakane, T.; Koike, I.; Yamamoto, T.; Sugiura, Y.; Harada, E.; Sugase, K.; Shimamura, T.; Ohmura, M.; Muraoka, K.; Yamamoto, A.; et al., Haem-dependent dimerization of PGRMC1/Sigma-2 receptor facilitates cancer proliferation and chemoresistance. *Nature communications* **2016,** *7*, 11030 `
13. McGuire, M. R.; Mukhopadhyay, D.; Myers, S. L.; Mosher, E. P.; Brookheart, R. T.; Kammers, K.; Sehgal, A.; Selen, E. S.; Wolfgang, M. J.; Bumpus, N. N., Progesterone receptor membrane component

1 (PGRMC1) binds and stabilizes cytochromes P450 through a heme-independent mechanism. *Journal of Biological Chemistry* **2021,** *297* (5), 101316.
14. McGuire, M. R.; Espenshade, P. J., PGRMC1: An enigmatic heme-binding protein. *Pharmacology & Therapeutics* **2022**, 108326.
15. Lösel, R. M.; Besong, D.; Peluso, J. J.; Wehling, M., Progesterone receptor membrane component 1—many tasks for a versatile protein. *Steroids* **2008,** *73* (9-10), 929-934.
16. Jakszyn, P.; Luján-Barroso, L.; Agudo, A.; Bueno-de-Mesquita, H. B.; Molina, E.; Sánchez, M. J.; Fonseca-Nunes, A.; Siersema, P. D.; Matiello, A.; Tumino, R., Meat and heme iron intake and esophageal adenocarcinoma in the European Prospective Investigation into Cancer and Nutrition study. *International journal of cancer* **2013,** *133* (11), 2744-2750.
17. Bastide, N. M.; Pierre, F. H.; Corpet, D. E., Heme iron from meat and risk of colorectal cancer: a meta-analysis and a review of the mechanisms involved. *Cancer prevention research* **2011,** *4* (2), 177-184.
18. Asperger, H.; Stamm, N.; Gierke, B.; Pawlak, M.; Hofmann, U.; Zanger, U. M.; Marton, A.; Katona, R. L.; Buhala, A.; Vizler, C., Progesterone receptor membrane component 1 regulates lipid homeostasis and drives oncogenic signaling resulting in breast cancer progression. *Breast Cancer Research* **2020,** *22* (1), 1-16.
19. Ahmed, I. S.; Chamberlain, C.; Craven, R. J., S2rpgrmc1: the cytochrome-related sigma-2 receptor that regulates lipid and drug metabolism and hormone signaling. *Expert opinion on drug metabolism & toxicology* **2012,** *8* (3), 361-370.
20. Ahmed, I. S.; Rohe, H. J.; Twist, K. E.; Mattingly, M. N.; Craven, R. J., Progesterone receptor membrane component 1 (Pgrmc1): a heme-1 domain protein that promotes tumorigenesis and is inhibited by a small molecule. *Journal of Pharmacology and Experimental Therapeutics* **2010,** *333* (2), 564-573.
21. Mallory, J. C.; Crudden, G.; Johnson, B. L.; Mo, C.; Pierson, C. A.; Bard, M.; Craven, R. J., Dap1p, a heme-binding protein that regulates the cytochrome P450 protein Erg11p/Cyp51p in Saccharomyces cerevisiae. *Molecular and cellular biology* **2005,** *25* (5), 1669-1679.
22. Li, J.; Lee, A. S., Stress induction of GRP78/BiP and its role in cancer. *Current molecular medicine* **2006,** *6* (1), 45-54.
23. Craven, R. J.; Mallory, J. C.; Hand, R. A., Regulation of iron homeostasis mediated by the heme-binding protein Dap1 (damage resistance protein 1) via the P450 protein Erg11/Cyp51. *Journal of biological chemistry* **2007,** *282* (50), 36543-36551.
24. Izzo, N. J.; Xu, J.; Zeng, C.; Kirk, M. J.; Mozzoni, K.; Silky, C.; Rehak, C.; Yurko, R.; Look, G.; Rishton, G., Alzheimer's therapeutics targeting amyloid beta 1–42 oligomers II: Sigma-2/PGRMC1 receptors mediate Abeta 42 oligomer binding and synaptotoxicity. *PloS one* **2014,** *9* (11), e111899.
25. Szczesna-Skorupa, E.; Kemper, B., Progesterone Receptor Membrane Component 1 Inhibits the Activity of Drug-Metabolizing Cytochromes P450 and Binds to Cytochrome P450 Reductase. *MOLECULAR PHARMACOLOGY* **2010,** *79* (3), 340-350.
26. Yasuaki Kabe, H. H. a. M. S., Function and structural regulation of the carbon monoxide (CO)responsive membrane protein PGRMC1. *Journal of Clinical Biochemistry and Nutrition* **2018,** *63* (1), 12-17.
27. Pedroza, D. A.; Rajamanickam, V.; Subramani, R.; Bencomo, A.; Galvez, A.; Lakshmanaswamy, R., Progesterone receptor membrane component 1 promotes the growth of breast cancers by altering the phosphoproteome and augmenting EGFR/PI3K/AKT signalling. *British journal of cancer* **2020,** *123* (8), 1326-1335.
28. Pedroza, D. A.; Subramani, R.; Tiula, K.; Do, A.; Rashiraj, N.; Galvez, A.; Chatterjee, A.; Bencomo, A.; Rivera, S.; Lakshmanaswamy, R., Crosstalk between progesterone receptor membrane component 1 and estrogen receptor α promotes breast cancer cell proliferation. *Laboratory Investigation* **2021,** *101* (6), 733-744.
29. Xu, X.; Ruan, X.; Zhang, Y.; Cai, G.; Ju, R.; Yang, Y.; Cheng, J.; Gu, M., Comprehensive analysis of the implication of PGRMC1 in triple-negative breast cancer. *Frontiers in Bioengineering and Biotechnology* **2021,** *9*, 714030.

30. Lee, S. K.; Kweon, Y. C.; Lee, A. R.; Lee, Y. Y.; Park, C. Y., Metastasis enhancer PGRMC1 boosts store-operated Ca2+ entry by uncoiling Ca2+ sensor STIM1 for focal adhesion turnover and actomyosin formation. *Cell Reports* **2022,** *38* (3), 110281.
31. Shih, C.-C.; Chou, H.-C.; Chen, Y.-J.; Kuo, W.-H.; Chan, C.-H.; Lin, Y.-C.; Liao, E.-C.; Chang, S.-J.; Chan, H.-L., Role of PGRMC1 in cell physiology of cervical cancer. *Life sciences* **2019,** *231*, 116541.
32. Krissinel, E.; Henrick, K., Inference of macromolecular assemblies from crystalline state. *Journal of molecular biology* **2007,** *372* (3), 774-797.
33. Piel III, R. B.; Shiferaw, M. T.; Vashisht, A. A.; Marcero, J. R.; Praissman, J. L.; Phillips, J. D.; Wohlschlegel, J. A.; Medlock, A. E., A novel role for progesterone receptor membrane component 1 (PGRMC1): a partner and regulator of ferrochelatase. *Biochemistry* **2016,** *55* (37), 5204-5217.
34. Raran-Kurussi, S.; Cherry, S.; Zhang, D.; Waugh, D. S., Removal of affinity tags with TEV protease. In *Heterologous Gene Expression in E. coli*, Springer: 2017; pp 221-230.
35. Liu, Y.; Moënne-Loccoz, P.; Hildebrand, D. P.; Wilks, A.; Loehr, T. M.; Mauk, A. G.; Ortiz de Montellano, P. R., Replacement of the proximal histidine iron ligand by a cysteine or tyrosine converts heme oxygenase to an oxidase. *Biochemistry* **1999,** *38* (12), 3733-3743.
36. Nagatomo, S.; Jin, Y.; Nagai, M.; Hori, H.; Kitagawa, T., Changes in the abnormal α-subunit upon CO-binding to the normal β-subunit of Hb M Boston: resonance Raman, EPR and CD study. *Biophysical chemistry* **2002,** *98* (1-2), 217-232.
37. Nagatomo, S.; Shoji, M.; Terada, T.; Nakatani, K.; Shigeta, Y.; Hirota, S.; Yanagisawa, S.; Kubo, M.; Kitagawa, T.; Nagai, M., Heme-bound tyrosine vibrations in hemoglobin M: Resonance Raman, crystallography, and DFT calculation. *Biophysical Journal* **2022,** *121* (14), 2767-2780.
38. Mokry, D. Z.; Nadia-Albete, A.; Johnson, M. K.; Lukat-Rodgers, G. S.; Rodgers, K. R.; Lanzilotta, W. N., Spectroscopic evidence for a 5-coordinate oxygenic ligated high spin ferric heme moiety in the Neisseria meningitidis hemoglobin binding receptor. *Biochimica et Biophysica Acta (BBA)-General Subjects* **2014,** *1840* (10), 3058-3066.
39. Grigg, J. C.; Mao, C. X.; Murphy, M. E., Iron-coordinating tyrosine is a key determinant of NEAT domain heme transfer. *Journal of molecular biology* **2011,** *413* (3), 684-698.
40. Nygaard, T. K.; Liu, M.; McClure, M. J.; Lei, B., Identification and characterization of the heme-binding proteins SeShp and SeHtsA of Streptococcus equi subspecies equi. *BMC microbiology* **2006,** *6* (1), 1-10.
41. Eakanunkul, S.; Lukat-Rodgers, G. S.; Sumithran, S.; Ghosh, A.; Rodgers, K. R.; Dawson, J. H.; Wilks, A., Characterization of the periplasmic heme-binding protein shut from the heme uptake system of Shigella dysenteriae. *Biochemistry* **2005,** *44* (39), 13179-13191.
42. Yukl, E. T.; Jepkorir, G.; Alontaga, A. Y.; Pautsch, L.; Rodriguez, J. C.; Rivera, M.; Moënne-Loccoz, P., Kinetic and spectroscopic studies of hemin acquisition in the hemophore HasAp from Pseudomonas aeruginosa. *Biochemistry* **2010,** *49* (31), 6646-6654.
43. Arnoux, P.; Haser, R.; Izadi, N.; Lecroisey, A.; Delepierre, M.; Wandersman, C.; Czjzek, M., The crystal structure of HasA, a hemophore secreted by Serratia marcescens. *Nature structural biology* **1999,** *6* (6), 516-520.
44. Giovannetti, R., The use of spectrophotometry UV-Vis for the study of porphyrins. *Macro to nano spectroscopy* **2012**, 87-108.
45. Gouterman, M., Study of the Effects of Substitution on the Absorption Spectra of Porphin. *The Journal of Chemical Physics* **1959,** *30* (5), 1139-1161.
46. Gouterman, M., Spectra of porphyrins. *Journal of Molecular Spectroscopy* **1961,** *6*, 138-163.
47. Gouterman, M.; Wagnière, G. H.; Snyder, L. C., Spectra of porphyrins: Part II. Four orbital model. *Journal of Molecular Spectroscopy* **1963,** *11* (1-6), 108-127.
48. Weiss, C.; Kobayashi, H.; Gouterman, M., Spectra of porphyrins: Part III. Self-consistent molecular orbital calculations of porphyrin and related ring systems. *Journal of Molecular Spectroscopy* **1965,** *16* (2), 415-450.
49. Rodger, A.; Marrington, R.; Roper, D.; Windsor, S., Circular dichroism spectroscopy for the study of protein-ligand interactions. *Protein-ligand interactions: methods and applications* **2005**, 343-363.

50. Daviter, T.; Chmel, N.; Rodger, A., Circular and linear dichroism spectroscopy for the study of protein–ligand interactions. *Protein-ligand interactions: methods and applications* **2013**, 211-241.
51. Abriata, L. A., A simple spreadsheet program to simulate and analyze the far-UV circular dichroism spectra of proteins. *Journal of Chemical Education* **2011,** *88* (9), 1268-1273.
52. Correa, D.; Ramos, C. H. I., The use of circular dichroism spectroscopy to study protein folding, form and function. *African Journal of Biochemistry Research* **2009,** *3* (5), 164-173.
53. Krieger, E.; Vriend, G., YASARA View—molecular graphics for all devices—from smartphones to workstations. *Bioinformatics* **2014,** *30* (20), 2981-2982.
54. Land, H.; Humble, M. S., YASARA: a tool to obtain structural guidance in biocatalytic investigations. *Protein engineering: methods and protocols* **2018**, 43-67.
55. Teale, F.; Weber, G., Ultraviolet fluorescence of the aromatic amino acids. *Biochemical Journal* **1957,** *65* (3), 476.
56. Ghisaidoobe, A. B.; Chung, S. J., Intrinsic tryptophan fluorescence in the detection and analysis of proteins: a focus on Förster resonance energy transfer techniques. *International journal of molecular sciences* **2014,** *15* (12), 22518-22538.
57. Möller, M.; Denicola, A., Protein tryptophan accessibility studied by fluorescence quenching. *Biochemistry and Molecular Biology Education* **2002,** *30* (3), 175-178.
58. Möller, M.; Denicola, A., Study of protein-ligand binding by fluorescence. *Biochemistry and Molecular Biology Education* **2002,** *30* (5), 309-312.
59. Yammine, A.; Gao, J.; Kwan, A. H., Tryptophan fluorescence quenching assays for measuring protein-ligand binding affinities: principles and a practical guide. *Bio-protocol* **2019,** *9* (11), e3253-e3253.
60. Yonetani, T.; Drott, H. R.; Leigh Jr, J. S.; Reed, G. H.; Waterman, M. R.; Asakura, T., Electromagnetic Properties of Hemoproteins: III. Electron Paramagnetic Resonance Characteristics of Iron (III) and Manganese (II) Protoporphyrins IX and Their Apohemoprotein Complexes in High Spin States. *Journal of Biological Chemistry* **1970,** *245* (11), 2998-3003.
61. Blumberg, W.; Peisach, J.; Wittenberg, B. A.; Wittenberg, J. B., The electronic structure of protoheme proteins: I. An electron paramagnetic resonance and optical study of horseradish peroxidase and its derivatives. *Journal of Biological Chemistry* **1968,** *243* (8), 1854-1862.
62. Tsai, A.; Kulmacz, R.; Wang, J.-S.; Wang, Y.; Van Wart, H.; Palmer, G., Heme coordination of prostaglandin H synthase. *Journal of Biological Chemistry* **1993,** *268* (12), 8554-8563.
63. Desta, I. T.; Porter, K. A.; Xia, B.; Kozakov, D.; Vajda, S., Performance and its limits in rigid body protein-protein docking. *Structure* **2020,** *28* (9), 1071-1081. e3.
64. Wittenberg, B. A.; Kampa, L.; Wittenberg, J. B.; Blumberg, W.; Peisach, J., The electronic structure of protoheme proteins: II. An electron paramagnetic resonance and optical study of cytochrome c peroxidase and its derivatives. *Journal of Biological Chemistry* **1968,** *243* (8), 1863-1870.
65. Schmid, M.; Prinz, T. K.; Stäbler, A.; Sängerlaub, S., Effect of sodium sulfite, sodium dodecyl sulfate, and urea on the molecular interactions and properties of whey protein isolate-based films. *Frontiers in chemistry* **2017,** *4*, 49.
66. Neubauer, H.; Clare, S. E.; Wozny, W.; Schwall, G. P.; Poznanović, S.; Stegmann, W.; Vogel, U.; Sotlar, K.; Wallwiener, D.; Kurek, R., Breast cancer proteomics reveals correlation between estrogen receptor status and differential phosphorylation of PGRMC1. *Breast Cancer Research* **2008,** *10* (5), 1-16.
67. Kozakov, D.; Beglov, D.; Bohnuud, T.; Mottarella, S. E.; Xia, B.; Hall, D. R.; Vajda, S., How good is automated protein docking? *Proteins: Structure, Function, and Bioinformatics* **2013,** *81* (12), 2159-2166.
68. Kozakov, D.; Hall, D. R.; Xia, B.; Porter, K. A.; Padhorny, D.; Yueh, C.; Beglov, D.; Vajda, S., The ClusPro web server for protein–protein docking. *Nature protocols* **2017,** *12* (2), 255-278.
69. Vajda, S.; Yueh, C.; Beglov, D.; Bohnuud, T.; Mottarella, S. E.; Xia, B.; Hall, D. R.; Kozakov, D., New additions to the C lus P ro server motivated by CAPRI. *Proteins: Structure, Function, and Bioinformatics* **2017,** *85* (3), 435-444.

70. Pettway, Y. D.; Neder, T. H.; Ho, D. H.; Fox, B. M.; Burch, M.; Colson, J.; Liu, X.; Kellum, C. E.; Hyndman, K. A.; Pollock, J. S., Early life stress induces dysregulation of the heme pathway in adult mice. *Physiological Reports* **2021,** *9* (10), e14844.
71. Hooda, J.; Shah, A.; Zhang, L., Heme, an essential nutrient from dietary proteins, critically impacts diverse physiological and pathological processes. Nutrients 2014; 6: 1080-1102. 2019.